

Tight-binding analysis of the electronic structure of dilute bismide alloys of GaP and GaAsMuhammad Usman,^{1,*} Christopher A. Broderick,^{1,2} Andrew Lindsay,¹ and Eoin P. O'Reilly^{1,2}¹*Tyndall National Institute, Lee Maltings, Dyke Parade, Cork, Ireland*²*Department of Physics, University College Cork, Cork, Ireland*

(Received 22 June 2011; revised manuscript received 19 September 2011; published 9 December 2011)

We develop an atomistic, nearest-neighbor sp^3s^* tight-binding Hamiltonian to investigate the electronic structure of dilute bismide alloys of GaP and GaAs. Using this model, we calculate that the incorporation of dilute concentrations of Bi in GaP introduces Bi-related defect states in the band gap, which interact with the host matrix valence band edge via a Bi composition dependent band anticrossing (BAC) interaction. By extending this analysis to $\text{GaBi}_x\text{As}_{1-x}$, we demonstrate that the observed strong variation of the band gap (E_g) and spin-orbit-splitting energy (Δ_{SO}) with Bi composition can be well explained in terms of a BAC interaction between the extended states of the GaAs valence band edge and highly localized Bi-related defect states lying in the valence band, with the change in E_g also having a significant contribution from a conventional alloy reduction in the conduction band edge energy. Our calculated values of E_g and Δ_{SO} are in good agreement with experiment throughout the investigated composition range ($x \leq 13\%$). In particular, our calculations reproduce the experimentally observed crossover to an $E_g < \Delta_{\text{SO}}$ regime at approximately 10.5% Bi composition in bulk $\text{GaBi}_x\text{As}_{1-x}$. Recent x-ray spectroscopy measurements have indicated the presence of Bi pairs and clusters even for Bi compositions as low as 2%. We include a systematic study of different Bi nearest-neighbor environments in the alloy to achieve a quantitative understanding of the effect of Bi pairing and clustering on the $\text{GaBi}_x\text{As}_{1-x}$ electronic structure.

DOI: [10.1103/PhysRevB.84.245202](https://doi.org/10.1103/PhysRevB.84.245202)

PACS number(s): 61.43.Dq

I. INTRODUCTION

Highly mismatched semiconductor alloys such as $\text{GaN}_x\text{As}_{1-x}$ have attracted considerable interest both from a fundamental perspective and also because of their potential device applications.¹⁻⁴ When a small fraction of As is replaced by N in GaAs, the band gap (E_g) initially decreases rapidly, by ≈ 150 meV when 1% of As is replaced by N.^{5,6} Similar behavior has been experimentally observed in $\text{GaBi}_x\text{As}_{1-x}$, where E_g has been observed to initially decrease by 90 meV (Refs. 7-10) per percent of Bi replacing As in the alloy. In addition to this, recent experiments^{11,12} have also revealed the presence of a large bowing of the spin-orbit-splitting energy (Δ_{SO}) with increasing Bi composition.

It has been recently shown¹³ that, by increasing the Bi composition in $\text{GaBi}_x\text{As}_{1-x}$ to $\approx 11\%$, we enter an $E_g < \Delta_{\text{SO}}$ regime in the alloy. This regime is of interest for the design of highly efficient optoelectronic devices since it opens up the possibility of suppression of the nonradiative Auger recombination process involving excitation of holes from the highest valence band into the spin-orbit split-off band, a loss mechanism that plagues the efficiency and dominates the threshold current in III-V multinary lasers operating in the telecommunication wavelength range.¹³

The band gap reduction in $\text{GaN}_x\text{As}_{1-x}$ has been explained using a band anticrossing (BAC) model.^{5,6} It is well established that replacing a single As atom by N introduces a resonant defect level above the conduction band edge (CBE) in GaAs. This occurs because N is considerably more electronegative and is also 40% smaller than As. The interaction between the resonant N states and the CBE of the host GaAs matrix then accounts for the observed rapid reduction in E_g .

It has been proposed that replacing As by Bi could introduce a similar BAC effect.⁷ Like N and As, Bi is also a group-V element, which lies below Sb in the periodic table. Bi is

much larger than As, and is also less electronegative. It should therefore be expected that any Bi-related resonant defect levels should lie in the valence band (VB) and that, if an anticrossing interaction occurs, it will occur between the Bi-related defect level and the valence band edge (VBE) of the GaAs matrix.

Recent x-ray absorption spectroscopy analysis of $\text{GaBi}_x\text{As}_{1-x}$ (Ref. 14) revealed that Bi atoms tend to form pairs and clusters in the alloy for $x \gtrsim 2\%$. For this reason, it is also of interest to explore the impact of Bi pairs and Bi clusters on the electronic structure of $\text{GaBi}_x\text{As}_{1-x}$. Such analysis requires atomistic modeling of the alloy since continuum methods such as the $\mathbf{k} \cdot \mathbf{p}$ and effective mass approximations are unable to predict the influence of such pairs and clusters on the electronic structure.

Although there is an increasing experimental interest in the structural^{14,15} and electronic^{7-9,11,16} properties of $\text{GaBi}_x\text{As}_{1-x}$, there have been comparatively few theoretical studies to date of this extreme semiconductor alloy. Previous theoretical investigations have employed the LDA + C,^{17,18} $\mathbf{k} \cdot \mathbf{p}$,⁷ and empirical pseudopotential¹⁹ methods. These theoretical approaches have provided a range of insights, but it remains controversial as to whether the observed reduction in energy gap is due to an anticrossing interaction¹⁶ or is better explained using more conventional alloy and disorder models.¹⁷

The LDA + C calculations of Janotti *et al.*¹⁸ presented the first band structure calculations of GaBi, and initial investigations of the influence of Bi on the electronic structure of $\text{GaBi}_x\text{As}_{1-x}$. Zhang *et al.*¹⁹ presented pseudopotential calculations that were in good agreement with the experimentally measured values of E_g and Δ_{SO} over the small composition range considered ($x \leq 4\%$). They also identified a Bi-related resonant defect state E_{Bi} , which they found to lie 80 meV below the GaAs VBE in the dilute doping limit. The best

choice of model to describe the influence of such a resonant level on the band structure has recently been discussed by Deng *et al.*,¹⁷ who argued that it was not appropriate to use the BAC model to describe the impact of Bi incorporation, and proposed instead the use of a band-broadening picture.

We find here a Bi-related level below the GaAs VBE in $\text{GaBi}_x\text{As}_{1-x}$, in agreement with previous work. Our comparative calculations of $\text{GaBi}_x\text{P}_{1-x}$ and $\text{GaBi}_x\text{As}_{1-x}$ confirm an anticrossing interaction between the Bi-related resonant state and the VBE. We also investigate the influence of Bi pair and cluster states on the electronic structure, showing that these pairs and clusters give rise to additional energy levels, which tend to move into the energy gap with increasing cluster size, analogous to the behavior of N pair and cluster levels in GaAs (Ref. 20) and GaP.²¹

The $\mathbf{k} \cdot \mathbf{p}$ calculations of Alberi *et al.*⁷ include explicitly BAC interactions between the GaAs VBE and lower-lying Bi-related levels in order to fit the experimentally observed variation of E_g for dilute Bi compositions. They also propose a second BAC interaction between the GaAs spin split-off (SO) band and a Bi-related SO defect level, 1.9 eV below the GaAs VBE. The inclusion of such a level would necessarily produce a BAC-induced upward shift in the SO band-edge energy E_{SO} . We find in our calculations that the evolution of the spin-split-off band is well described using a conventional alloy model, without the need to include such an SO-related BAC interaction.

We have previously demonstrated that a parametrized tight-binding (TB) approach provides an accurate and versatile method to analyze the electronic structure of highly mismatched semiconductor alloys such as $\text{GaN}_x\text{As}_{1-x}$, $\text{GaBi}_x\text{P}_{1-x}$, and $\text{GaBi}_x\text{As}_{1-x}$. Since a basis of localized states is employed, it is possible using the TB method to probe explicitly and quantitatively the effect of an isolated impurity atom (e.g., replacing a single As atom by either N or Bi in GaAs) on the host matrix electronic structure.²²⁻²⁴ The sp^3s^* TB Hamiltonian developed for dilute nitride alloys²⁵ fully accounts for a wide range of experimental data, and also gives results in good agreement with pseudopotential calculations.²⁰ We present here an sp^3s^* TB Hamiltonian to calculate the electronic structure of dilute bismide alloys of GaP and GaAs. This Hamiltonian gives good agreement with pseudopotential and LDA + C calculations¹⁹ and with experiment over the full composition range investigated ($x \leq 13\%$).

We start our calculations with the study of ordered $\text{GaBi}_x\text{As}_{1-x}$ and $\text{GaBi}_x\text{P}_{1-x}$ supercells. It is useful to include $\text{GaBi}_x\text{P}_{1-x}$ in our analysis because Bi is sufficiently different to P that it introduces defect states just above the VBE in GaP.²⁶ Since these Bi-related defect states are in the energy gap, it is then much easier to identify and follow the interaction between the VBE and these levels as a function of increasing Bi composition. Our calculations show clearly for $\text{GaBi}_x\text{P}_{1-x}$ that there is an anticrossing interaction between the Bi defect states and the GaP VBE.²⁷

Having established that there is a BAC interaction in $\text{GaBi}_x\text{P}_{1-x}$, we then extend our calculations to consider ordered supercells of $\text{GaBi}_x\text{As}_{1-x}$. By comparison with $\text{GaBi}_x\text{P}_{1-x}$, we identify that there are Bi-related resonant

defect levels below the VBE in $\text{GaBi}_x\text{As}_{1-x}$ and that these resonant defect levels interact with and push the VBE up in energy through an anticrossing interaction. The effect of the resonant levels has been confirmed in $\text{GaN}_x\text{As}_{1-x}$ through photoreflectance (PR) measurements, which show a higher energy feature E_+ associated with transitions to the resonant level.^{5,28,29} We show that, because of the large density of valence states, it is not possible to experimentally identify similar higher-energy transitions at any Bi composition in $\text{GaBi}_x\text{As}_{1-x}$.

Next, we investigate the effect of Bi pairs and clusters in $\text{GaBi}_x\text{As}_{1-x}$ alloys by placing a single pair or cluster in a large (4096-atom) supercell in order to investigate its effect on the electronic structure. Our calculations highlight the evolution of the defect energy levels and their interaction with the VBE with increasing cluster size. This analysis later aids our understanding of the calculated electronic properties of randomly disordered $\text{GaBi}_x\text{As}_{1-x}$ supercells, in which the number of Bi pairs increases as x^2 and the number of n -atom clusters increases as x^n .

Having established an understanding of the evolution of the Bi resonant state in ordered supercells containing only a single Bi atom, single Bi pair, or small Bi cluster, we next present calculations of disordered 4096-atom $\text{GaBi}_x\text{As}_{1-x}$ supercells with larger Bi compositions ($x \leq 13\%$). In such systems, we find that the CBE energy decreases both linearly and rapidly with increasing Bi composition, so that the experimentally observed reduction in the band gap is then due both to a BAC interaction in the VB and to conventional alloy behavior in the conduction band (CB). In addition, our calculations indicate that the observed strong bowing of the SO-splitting energy^{11,12} is predominantly attributable to the upward shift in the $\text{GaBi}_x\text{As}_{1-x}$ VBE with Bi composition, with a minor contribution from a downward shift in E_{SO} , which is linear in Bi composition and, hence, well understood as a conventional alloying effect. This linear variation in E_{SO} is contrary to the SO-BAC interaction included in the $\mathbf{k} \cdot \mathbf{p}$ Hamiltonian introduced by Alberi *et al.*⁷ and shows that the Bi-related resonant state introduced in the VB interacts solely with the GaAs VBE at the Brillouin zone center (Γ point).

Our calculations accurately reproduce the experimentally observed¹¹ crossing of the band gap and the SO-splitting energies at a Bi composition of $\approx 10.5\%$ in the alloy. Our analysis therefore lends support to the experimental conclusion that $\text{GaBi}_x\text{As}_{1-x}$ alloys can be used to obtain emission in the technologically important 1.3- and 1.5- μm wavelength ranges on a GaAs substrate, while also demonstrating that the unusual material behavior present in the alloy can be understood simply in terms of a BAC interaction.

The remainder of this paper is organized as follows: In Sec. II, we give a detailed presentation of the TB Hamiltonian and calculation procedure. In Sec. III A, we apply the TB model to explore in detail the electronic structure of dilute ordered bismide alloys of GaP and GaAs, beginning with $\text{GaBi}_x\text{P}_{1-x}$. Following this, we continue our analysis of $\text{GaBi}_x\text{As}_{1-x}$ by performing a systematic study of the effects of Bi pairing and clustering on the electronic structure in Sec. III B. We then consider disordered $\text{GaBi}_x\text{P}_{1-x}$ supercells

in Sec. III C and disordered $\text{GaBi}_x\text{As}_{1-x}$ supercells in Sec. III D. Finally, we present our conclusions in Sec. IV.

II. METHODOLOGY

A. sp^3s^* tight-binding model

We use an sp^3s^* nearest-neighbor tight-binding Hamiltonian including spin-orbit coupling to investigate the electronic structure of the different alloys. The interatomic interaction parameters vary with bond length and the magnitude of the onsite parameters depends explicitly on the overall neighbor environment.²⁵

The alloy band structure calculations are undertaken using the NanoElectronic MOdeling (NEMO 3-D) simulator.^{30–32} NEMO 3-D is a fully atomistic simulator and its capabilities include modeling of realistic multimillion atom geometries for embedded quantum dot devices,^{33–35} strained disordered quantum wells,³⁶ and single impurities in Si FinFET structures.³⁷

In our sp^3s^* model, the onsite orbital energies for a given atom are determined by taking the average of the values from the binary compounds formed by that atom and its four nearest neighbors, taking into account the relevant valence band offsets (VBOs). The interatomic interaction energies are taken to vary with bond length d as $(\frac{d_0}{d})^\eta$, where d_0 is the equilibrium bond length in the equivalent binary compound, and η is a scaling parameter, the magnitude of which depends on the type of interaction being considered. The scaling indices for GaP and GaAs are determined by fitting the bond length dependence of their nearest-neighbor interaction parameters to a range of hydrostatic deformation potentials.²³ Since there are no experimental or theoretical deformation potentials available for GaBi, the scaling indices for GaBi were adapted from those of GaAs. We modify the GaAs η values, in particular for the p states, in order to ensure that Bi gives a defect state in the energy gap of GaP, as observed experimentally.²⁶ These modified values of η for GaBi then give a Bi resonant state inside the valence band of GaAs for GaBiAs, consistent with earlier pseudopotential calculations.¹⁹ The effects of changes in bond angle are taken into account through the two-center integral expressions of Slater and Koster.³⁸

The self-energies and interatomic interaction parameters for the different binary compounds are listed in Table I. The parameters for GaAs and GaP are based on those that we have used previously when studying $\text{GaN}_x\text{As}_{1-x}$ (Ref. 25) and $\text{GaN}_x\text{P}_{1-x}$,²¹ but we now include spin-orbit interactions. The parameters for GaBi were obtained by fitting to LDA + C calculations.¹⁸ Figure 1 shows the bulk GaBi band structure obtained from our sp^3s^* Hamiltonian, compared with the LDA + C calculations of Janotti *et al.*¹⁸

The valence band offsets for GaAs and GaP are taken from Ref. 39. Since the binary compound GaBi has yet to be isolated, we need to estimate a value for the GaBi VBO. A VBO of 1.1 eV for GaBi was estimated by an extrapolation of the VBO as a function of lattice parameter (a) for Ga-containing III-V semiconductor binaries (see Fig. 2). This differs from the value of 0.8 eV used earlier by Alberi *et al.*,⁷ which appears to have been estimated by a linear extrapolation of VBO against the lattice parameter for GaN and GaP only. The scaling exponents η used to describe the variation of the

TABLE I. Lattice constants, orbital self-energies, interatomic interaction parameters, spin-orbit couplings, and valence band offsets for GaP, GaAs, and GaBi in the sp^3s^* Hamiltonian. Lattice constants are given here in Å; all other values are in eV.

	GaP	GaAs	GaBi
a	5.4505	5.6532	6.328
$E_{s,a}$	-8.1124	-8.6336	-8.3774
$E_{s,c}$	-2.1976	-2.9474	-5.6126
$E_{p,a}$	1.0952	0.9252	-0.1256
$E_{p,c}$	4.0851	3.5532	1.694
$E_{s^*,a}$	8.4796	7.0914	6.1262
$E_{s^*,c}$	7.1563	6.2	5.8164
$ss\sigma$	-1.8727	-1.6835	-1.3425
$pp\sigma$	3.0989	2.9500	2.0003
$pp\pi$	-0.7424	-0.7420	-0.6354
$s_a p_c \sigma$	1.8500	2.3920	2.3567
$s_c p_a \sigma$	2.7312	2.4200	1.2025
$s_a^* p_c \sigma$	1.9998	2.0400	1.8051
$s_c^* p_a \sigma$	2.1882	1.7700	0.5100
λ_a	0.0666	0.405	2.0142
λ_c	0.1734	0.165	0.1152
VBO	-0.5	0	1.1

interatomic matrix elements with bond length are listed in Table II.

The TB calculations were carried out on supercells containing up to 4096 atoms using the NEMO 3-D simulator. For the disordered structures, $\text{Ga}_{2048}\text{Bi}_M\text{Y}_{2048-M}$ ($Y = \text{P}, \text{As}$) supercells were constructed by substituting Bi atoms at random Y sites on a GaY lattice and relaxing the crystal to its lowest-energy configuration using a parametrized valence force field (VFF) model, including anharmonic corrections⁴¹ to the Keating potential.⁴² The VFF parameters used are listed in Table III. The parameters for GaAs are those obtained by Lazarenkova,⁴¹ while those for GaP and GaBi were derived based on the expressions of Martin⁴³ and the elastic constants of Vurgaftman *et al.*³⁹ and Ferhat and Zaoui,¹⁵ respectively. It is worth noting that, in the $\text{GaBi}_x\text{As}_{1-x}$ case, relaxed Ga-Bi bond lengths from our model follow the same trend revealed

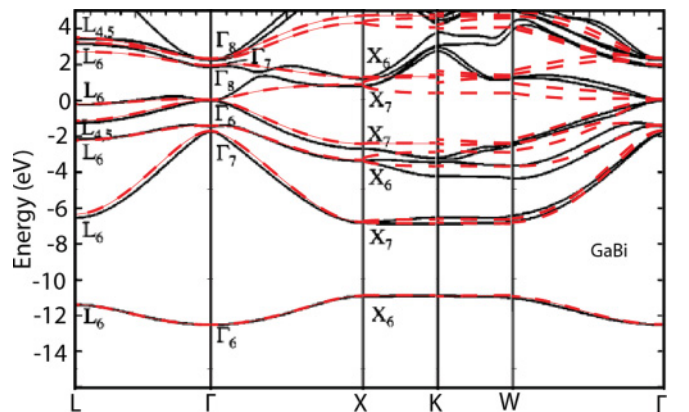


FIG. 1. (Color online) Bulk band structure of GaBi. The dashed red lines are the bands obtained from our sp^3s^* parametrization. The solid black lines are the LDA + C bands calculated by the authors of Ref. 18 (used with permission).

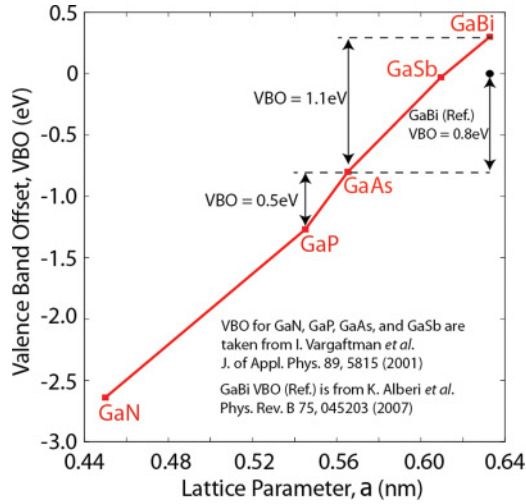


FIG. 2. (Color online) Valence band offset (VBO) as a function of lattice parameter for Ga-containing III-V semiconductor binaries. The values for GaN, GaP, GaAs, and GaSb are taken from Ref. 39. The GaBi VBO is estimated by extrapolating the trend to the GaBi lattice constant (6.328 Å) (Ref. 40). For comparison, the GaBi VBO value of 0.8 eV estimated by the authors of Ref. 7 is indicated by a black dot.

by x-ray absorption spectroscopy measurements,¹⁴ where we see a decreasing Ga-Bi bond length in the presence of Bi pairing and clustering, indicating increased localized strain in the alloy.

B. Tight-binding implementation of the band anticrossing model

The BAC model explains the extreme band gap bowing observed in $\text{Ga}(\text{In})\text{N}_x\text{As}_{1-x}$ in terms of an interaction between two levels, one at energy E_M associated with the extended CBE state $|\psi_{c,0}\rangle$ of the $\text{Ga}(\text{In})\text{As}$ matrix, and the other at energy E_D associated with the localized N impurity defect states $|\psi_N\rangle$, with the two states linked by a N-composition-dependent matrix element V_{DM} describing the interaction between them.⁵ The CBE energy of $\text{Ga}(\text{In})\text{N}_x\text{As}_{1-x}$ is then given by the lower eigenvalue E_- of the two-band Hamiltonian

$$\begin{pmatrix} E_D & V_{DM} \\ V_{DM} & E_M \end{pmatrix}. \quad (1)$$

A resonant feature associated with the upper eigenvalue E_+ of Eq. (1) has been observed in PR measurements,^{5,28,29} appearing in $\text{GaN}_x\text{As}_{1-x}$ for $x \gtrsim 0.2\%$ and remaining a relatively sharp feature until $x \approx 3\%$, beyond which composition it

TABLE II. Dimensionless scaling parameters η for the sp^3s^* interatomic interaction parameters in GaP, GaAs, and GaBi.

	GaP	GaAs	GaBi
$\eta_{ss\sigma}$	3.512	3.512	3.66
$\eta_{sp\sigma}$	4.3	4.3	4.08
$\eta_{pp\sigma}$	3.2042	3.2042	2.2
$\eta_{pp\pi}$	4.2357	4.2357	3.24
$\eta_{s^*p\sigma}$	5.5	5.5	5.5

TABLE III. VFF parameters and coefficients for anharmonic corrections to the Keating potential for unstrained, bulk GaP, GaAs, and GaBi. The VFF parameters α_0 and β_0 are in units of N m^{-1} . The anharmonicity constants A , B , and C are dimensionless.

	GaP	GaAs	GaBi
α_0	44.5	41.49	34.0
β_0	10.69	8.94	5.0
A	7.2	7.2	8.2
B	7.62	7.62	7.62
C	6.4	6.4	6.4

broadens and weakens, when the resonant state becomes degenerate with the large L -related conduction band density of states.⁴⁴ To investigate the resonant state $|\psi_N\rangle$ and its behavior, we used the sp^3s^* TB Hamiltonian to calculate the electronic structure of ordered $\text{GaN}_x\text{As}_{1-x}$ supercells.^{24,45} By comparing the calculated host and alloy CBE states $|\psi_{c,0}\rangle$ and $|\psi_{c,1}\rangle$ in large supercells ($\text{Ga}_{864}\text{N}_1\text{As}_{863}$ and $\text{Ga}_{864}\text{As}_{864}$, respectively), we derived the nitrogen resonant state $|\psi_N\rangle$, associated with an isolated N atom. In the BAC model, $|\psi_{c,1}\rangle$ is a linear combination of $|\psi_{c,0}\rangle$ and $|\psi_N\rangle$, with $|\psi_N\rangle$ then given by

$$|\psi_N\rangle = \frac{|\psi_{c,1}\rangle - \alpha|\psi_{c,0}\rangle}{\sqrt{1 - |\alpha|^2}}, \quad (2)$$

where $\alpha = \langle \psi_{c,0} | \psi_{c,1} \rangle$. The evolution of the conduction band structure in an ordered $\text{GaN}_x\text{As}_{1-x}$ supercell can then be very well described by associating a localized resonant state with each N atom in the supercell.²²

In the dilute bismide case, the BAC interaction is expected to occur in the valence band. Previous analysis⁷ has included a BAC interaction with each of the three doubly degenerate valence bands, namely, the heavy-hole (HH), light-hole (LH), and spin split-off (SO) bands. We find below that there is a BAC interaction with the HH and LH bands, but that there is no calculated BAC interaction involving the SO band. For dilute bismides, the Hamiltonian analogous to (1) is therefore

$$\begin{pmatrix} E_{\text{HH}} & 0 & V_{\text{Bi}} & 0 \\ 0 & E_{\text{LH}} & 0 & V_{\text{Bi}} \\ V_{\text{Bi}} & 0 & E_{\text{Bi}} & 0 \\ 0 & V_{\text{Bi}} & 0 & E_{\text{Bi}} \end{pmatrix}, \quad (3)$$

where $E_{\text{HH/LH}}$ are the (degenerate) host matrix VBE energies, E_{Bi} is the energy of the Bi-related resonant defect state, and $V_{\text{Bi}} = \beta\sqrt{x}$ is the composition-dependent interaction matrix element linking $E_{\text{HH/LH}}$ and E_{Bi} . For E_{Bi} above (below) the host matrix VBE, the interaction pushes down (up) the VBE.

Because of the four-fold degeneracy of the VBE states, we need to modify the approach used in Eq. (2) to determine the BAC interaction in $\text{GaBi}_x\text{Y}_{1-x}$ ($Y = \text{P, As}$). As a result of the HH/LH degeneracy, the calculated alloy VBE states each include an arbitrary admixture of the host matrix VBE states $|\psi_{l,0}\rangle$. We can therefore use the calculated alloy and host matrix TB wave functions to determine the four Bi resonant states $|\psi_{\text{Bi},i}\rangle$ as a linear combination of the $\text{GaBi}_x\text{Y}_{1-x}$ VBE,

$|\psi_{v,1,i}\rangle$, and $|\psi_{v,0,i}\rangle$, the part of the host (GaY) matrix VBE with which the i th Bi state $|\psi_{\text{Bi},i}\rangle$ interacts:

$$|\psi_{\text{Bi},i}\rangle = \frac{|\psi_{v,1,i}\rangle - \sum_{l=1}^4 |\psi_{l,0}\rangle \langle \psi_{l,0} | \psi_{v,1,i} \rangle}{\sqrt{1 - \sum_{l=1}^4 |\langle \psi_{l,0} | \psi_{v,1,i} \rangle|^2}} \quad (4)$$

in which the index l runs over the fourfold-degenerate levels of the GaY VBE.

In general, for an isolated Bi impurity, $|\psi_{\text{Bi},i}\rangle$ exhibits T_d symmetry so it will be fourfold degenerate, with energy E_{Bi} . We can calculate explicitly E_{Bi} and the interaction between $|\psi_{\text{Bi},i}\rangle$ and the GaY VBE β by calculating the appropriate matrix elements of the full TB Hamiltonian for the Bi-containing alloy \hat{H} for any one of the four degenerate Bi states:

$$E_{\text{Bi}} = \langle \psi_{\text{Bi}} | \hat{H} | \psi_{\text{Bi}} \rangle \quad (5)$$

$$\beta = \frac{V_{\text{Bi}}}{\sqrt{x}} = \frac{\langle \psi_{\text{Bi}} | \hat{H} | \psi_{v,0} \rangle}{\sqrt{x}}, \quad (6)$$

where $|\psi_{v,0,i}\rangle = \sum_{l=1}^4 |\psi_{l,0}\rangle \langle \psi_{l,0} | \psi_{v,1,i} \rangle$, with the sum again running over the fourfold-degenerate levels of the GaY VBE.

C. Calculation of fractional Γ character spectra in alloy supercells

In the ideal BAC model of Eqs. (1) and (3), the host matrix band-edge states are expected to mix in the alloy with the localized Bi-related defect states. In order to explore this BAC interaction, we calculate $G_{\Gamma}(E)$, which is the projection of the host matrix band-edge states onto the full spectrum of levels in the alloy supercell. In what follows, we use the subscripts $l,0$ and $k,1$ to index the unperturbed host and Bi-containing alloy states, respectively. The $G_{\Gamma}(E)$ spectrum is calculated by projecting the unperturbed Ga_NY_N ($Y = \text{P, As}$) Γ states $|\psi_{l,0}\rangle$ onto the spectrum for the $\text{Ga}_N\text{Bi}_M\text{Y}_{N-M}$ alloy supercell $\{E_k, |\psi_{k,1}\rangle\}$:

$$G_{\Gamma}(E) = \sum_k \sum_{l=1}^{g(E_l)} f_{\Gamma,kl} T(E_k - E), \quad (7)$$

$$f_{\Gamma,kl} = |\langle \psi_{k,1} | \psi_{l,0} \rangle|^2. \quad (8)$$

Here, we choose $T(E_k - E)$ as a ‘‘top hat’’ function of width 2 meV and unit height centered on E_k , and $g(E_l)$ is the degeneracy of the host (GaY) band having energy E_l at Γ [i.e., $g(E_l) = 2, 4$, and 2 for the conduction, valence, and SO bands, respectively].

We use $G_{\Gamma}(E)$ first to confirm the presence of a BAC interaction in ordered $\text{GaBi}_x\text{P}_{1-x}$ and $\text{GaBi}_x\text{As}_{1-x}$ structures, and then to analyze the effects of Bi pair and cluster states, as well as the evolution of the BAC interaction in disordered structures. We also use $G_{\Gamma}(E)$ to explore the evolution of the conduction and SO band edges in $\text{GaBi}_x\text{As}_{1-x}$ with Bi composition, showing that the variation in both cases is attributable to the conventional alloying effect. These calculations are discussed in detail in the next section.

III. RESULTS AND DISCUSSIONS

A. Bi state in ordered $\text{GaBi}_x\text{P}_{1-x}$ and $\text{GaBi}_x\text{As}_{1-x}$ supercells

1. $\text{Ga}_N\text{Bi}_1\text{P}_{N-1}$ supercells

We have found previously that it is straightforward to identify and analyze a band anticrossing interaction using Eqs. (4) to (7) in ordered supercell structures where the localized defect state is in the energy gap, as was the case for $\text{Ga}_N\text{P}_{1-x}$.²¹ It has been shown experimentally that an isolated Bi atom acts as an impurity in GaP, giving rise to a defect level ~ 100 meV above the VBE.²⁶ Our tight-binding model has been established to give a Bi defect state in the band gap of GaP, consistent with this experimental study. We therefore start our calculations by investigating the electronic structure of ordered $\text{Ga}_N\text{Bi}_1\text{P}_{N-1}$ supercells, in which a single substitutional Bi atom is inserted into the GaP matrix. Having established the main factors influencing the valence band structure in $\text{GaBi}_x\text{P}_{1-x}$, we then consider $\text{GaBi}_x\text{As}_{1-x}$, using the phosphide results to guide and support the interpretation of the arsenide calculations.

Figure 3 plots the fractional Γ character $G_{\Gamma}(E)$ associated with the GaP VBE states in $\text{Ga}_N\text{Bi}_1\text{P}_{N-1}$ supercells as the supercell size $2N$ ($x = N^{-1}$) decreases (increases) from Fig. 3(b) $N = 2048$ ($x = 0.049\%$) to Fig. 3(f) $N = 108$ ($x = 0.926\%$). For reference, we also include in Fig. 3(a) the calculated $G_{\Gamma}(E)$ for a pure GaP supercell, in which 100% of the HH/LH Γ character resides on the VBE.

When we replace a single P atom by Bi in a $\text{Ga}_{2048}\text{P}_{2048}$ supercell, we see in Fig. 3(b) that this gives rise to a fourfold-degenerate defect level, which lies above, and interacts with, the GaP VBE. The amplitude of the unperturbed GaP VBE states is distributed over two levels, corresponding to E_- and E_+ , as expected from the band anticrossing model of Eq. (3). We calculate using Eqs. (4) and (5) that the isolated Bi impurity

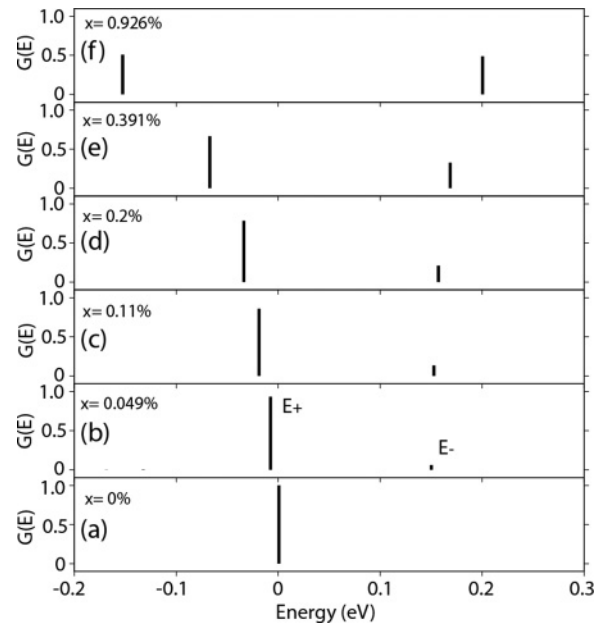


FIG. 3. Combined fractional HH/LH Γ character for a series of ordered $\text{Ga}_N\text{Bi}_1\text{P}_{N-1}$ supercells. The zero of energy is taken at the GaP VBE.

level lies 122 meV above the GaP VBE, and that each impurity state is highly localized, with 31% of its probability density localized on the Bi atom and the four nearest-neighbor Ga sites. We also calculate that the band anticrossing interaction V_{Bi} between the Bi-related defect levels E_{Bi} and the VBE is of magnitude $V_{\text{Bi}} = \beta\sqrt{x}$, with $\beta = 1.41$ eV. The calculated magnitude of the interaction parameter β in $\text{GaBi}_x\text{P}_{1-x}$ is then comparable to that which we have calculated previously²³ for $\text{GaN}_x\text{P}_{1-x}$ ($\beta = 1.74$ eV) and for $\text{GaN}_x\text{As}_{1-x}$ ($\beta = 2.00$ eV).

Having identified in this section that an anticrossing interaction does indeed occur between Bi-related defect levels and the GaP VBE in $\text{GaBi}_x\text{P}_{1-x}$, we now use this understanding to inform our analysis of the valence band structure of $\text{GaBi}_x\text{As}_{1-x}$.

2. $\text{Ga}_N\text{Bi}_1\text{As}_{N-1}$ supercells

Figure 4 plots the fractional Γ character $G_{\Gamma}(E)$ associated with the GaAs VBE states in $\text{Ga}_N\text{Bi}_1\text{As}_{N-1}$ supercells as the supercell size $2N$ (Bi composition, x) decreases (increases) from Fig. 4(b) $N = 2048$ ($x = 0.049\%$) to Fig. 4(f) $N = 108$ ($x = 0.926\%$). For reference, we again include as Fig. 4(a) the calculated $G_{\Gamma}(E)$ for a pure GaAs supercell, in which 100% of the HH/LH Γ character resides on the VBE.

We first consider a single substitutional Bi atom in a 4096-atom supercell [$x = 0.049\%$, Fig. 4(b)]. We see for this case that the HH and LH Γ character remains predominantly on the highest alloy valence states, with 98.2% of the Γ character on these states. Of the remaining 1.8%, 1.3% is found on a single energy state ≈ 117 meV below the GaAs VBE, with the other 0.5% spread over a series of lower-lying levels. Using Eq. (4), we identify that the state that mixes with each of the GaAs valence-band-edge states is a localized Bi resonant defect level, with very similar character to the localized defect state found in $\text{GaBi}_x\text{P}_{1-x}$. The Bi state is calculated to be

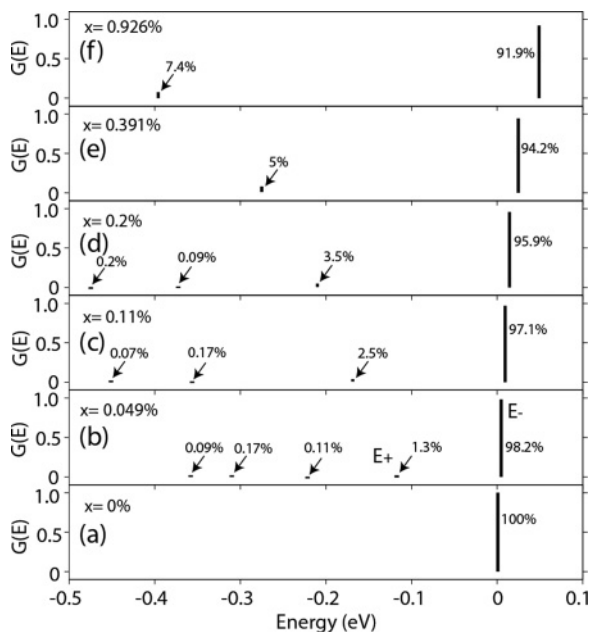


FIG. 4. Combined fractional HH/LH Γ character for a series of ordered $\text{Ga}_N\text{Bi}_1\text{As}_{N-1}$ supercells. The zero of energy is taken at the GaAs VBE.

highly localized, with 36% of its probability density localized on the Bi atom and the four nearest-neighbor Ga sites.

We calculate by evaluating $V_{\text{Bi}} = \langle \psi_{\text{Bi}} | \hat{H} | \psi_{v,0} \rangle$ for an isolated Bi impurity in a 4096-atom supercell that the band anticrossing interaction V_{Bi} between the Bi-related resonant defect level E_{Bi} and the GaAs VBE $E_{v,0}$ is of magnitude $V_{\text{Bi}} = \beta\sqrt{x}$, with $\beta = 1.13$ eV. The calculated magnitude of the interaction parameter β in $\text{GaBi}_x\text{As}_{1-x}$ is then smaller than the value in $\text{GaBi}_x\text{P}_{1-x}$, reflecting that there is less difference in electronegativity and size between a Bi and an As atom than there is between a Bi and a P atom.

When the size of the supercell is decreased from 4096 atoms to 216 atoms [Figs. 4(b)–4(f)], the interaction of the Bi-related resonant defect state with the GaAs VBE increases, thus pushing the valence band edge E_- upward in energy. The lower BAC level is pushed downward in energy and its fractional Γ character $G_{\Gamma}(E)$ also increases as a result of the increasing strength of the interaction. Overall, the Γ character associated with the lower BAC level is in all cases spread over several supercell levels [clearly visible in Figs. 4(b), 4(c), and 4(d), but running out of scale to lower energies in Figs. 4(e) and 4(f)], reflecting that the Bi states are resonant with a high density of host matrix valence band states.

Figure 5 shows the calculated values of β and E_{Bi} for a series of ordered $2N$ atom $\text{Ga}_N\text{Bi}_1\text{Y}_{N-1}$ ($Y = \text{P, As}$) supercells, where N is increased from 32 to 4000 atoms, retaining a cubic supercell at each N . Both the $\text{GaBi}_x\text{As}_{1-x}$ and

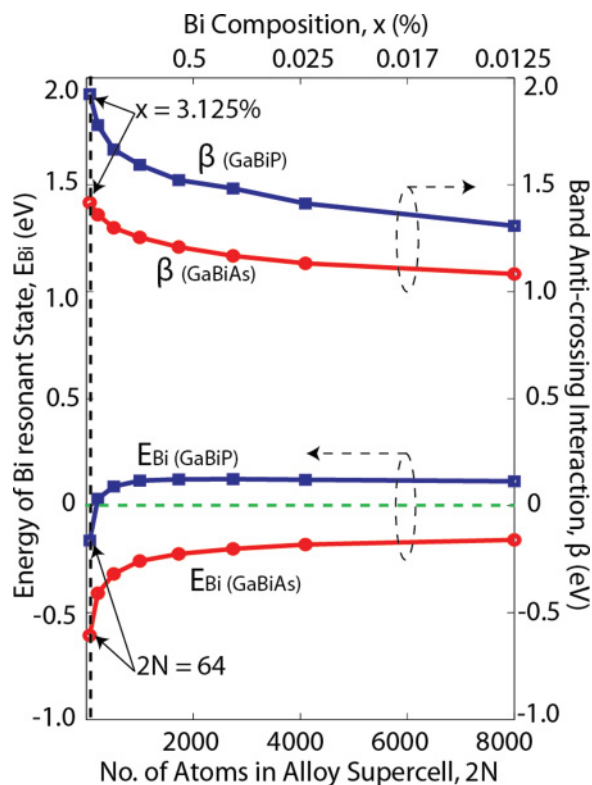


FIG. 5. (Color online) Plot of Bi resonant state energy E_{Bi} and band anticrossing parameter β as a function of the size of $\text{GaBi}_x\text{Y}_{1-x}$ ($Y = \text{P, As}$) supercell. Each supercell contains one Bi atom. The horizontal dotted line shows valence-band-edge energy in GaAs for $\text{GaBi}_x\text{As}_{1-x}$ and in GaP for $\text{GaBi}_x\text{P}_{1-x}$.

$\text{GaBi}_x\text{P}_{1-x}$ supercells exhibit similar trends. As the supercell size increases, the calculated strength of the band anticrossing interaction between the Bi impurity state and the GaAs VBE reduces. For larger supercells ($N > 2000$ atoms), we approach the dilute doping limit and the trend stabilizes. We also find that the calculated energy of the Bi resonant states E_{Bi} increases with increasing supercell size. The Bi impurity state is calculated to lie 607 meV below the GaAs VBE in a $\text{Ga}_{32}\text{Bi}_1\text{As}_{31}$ supercell, and its value increases to -0.18 eV in a $\text{Ga}_{4000}\text{Bi}_1\text{As}_{3999}$ supercell. This change arises due to the evolution of the GaY ($Y = \text{P}, \text{As}$) supercell zone center band structure with increasing supercell size. The GaY supercell zone center states form a complete set of basis states from which to construct the localized Bi states.⁴⁶ For the smallest (64-atom) supercell, the highest valence levels folded back to the zone center lie 1.45 eV (1.30 eV) below the VBE in GaAs (GaP). As the supercell size increases, more states get folded back with energies closer to the VBE. These states can be used to construct the Bi localized state energy, thus accounting for the calculated upward shift in the energy E_{Bi} with increasing supercell size. Based on the trends shown in Fig. 5, we predict values of approximately -0.18 and 1.13 eV for E_{Bi} and β for $\text{GaBi}_x\text{As}_{1-x}$ alloys in the dilute doping limit, respectively.

B. Bi pair and cluster states

Recent experimental investigations using x-ray absorption spectroscopy¹⁴ indicate that Bi atoms in dilute $\text{GaBi}_x\text{As}_{1-x}$ alloys tend to form localized pairs and clusters, even at relatively low Bi compositions. The presence of such pairs and clusters of N atoms has been observed in earlier studies on $\text{GaN}_x\text{As}_{1-x}$ alloys with dilute N concentrations,⁴⁷ and it has been shown that such pairs and clusters significantly affect the electronic structure of the alloy.^{20,48} We investigate here the impact of Bi pairs and clusters on the electronic structure of $\text{GaBi}_x\text{As}_{1-x}$.

We compare the electronic structure of seven different nearest-neighbor environments in a 4096-atom supercell: (i) a $\text{Ga}_{2048}\text{As}_{2048}$ supercell (Bi free), (ii) $\text{Ga}_{2048}\text{Bi}_1\text{As}_{2047}$

containing an isolated Bi atom, (iii) a $\text{Ga}_{2048}\text{Bi}_2\text{As}_{2046}$ supercell containing two isolated Bi atoms (where each Bi atom has no Bi belonging to either its first, second, or third shell of neighboring atoms), (iv) a $\text{Ga}_{2048}\text{Bi}_2\text{As}_{2046}$ supercell containing a pair of Bi atoms (i.e., a Ga atom having two Bi nearest neighbors), (v) a $\text{Ga}_{2048}\text{Bi}_3\text{As}_{2045}$ supercell containing three isolated Bi atoms [with each Bi atom satisfying the same isolation criterion as in (ii)], (vi) a $\text{Ga}_{2048}\text{Bi}_3\text{As}_{2045}$ supercell containing three Bi atoms forming a cluster, such that a single Ga atom has three Bi nearest neighbors (we shall henceforth refer to this nearest-neighbor environment as a cluster of type 1), and (vii) a $\text{Ga}_{2048}\text{Bi}_3\text{As}_{2045}$ supercell containing three Bi atoms forming a Bi-Ga-Bi-Ga-Bi chain, with the two Ga atoms in the chain each having two Bi nearest neighbors (this will be referred to as a cluster of type 2). The nearest-neighbor environments (iv), (vi), and (vii) are depicted in Figs. 6(a), 6(b), and 6(c), respectively.

From the relaxation of the supercell configurations described in (ii) to (vii), we calculate the average relaxed Ga-Bi bond length in each case. For a single Bi atom, the relaxed Ga-Bi bond length is 2.647 Å. When we introduce a Bi pair, the Bi-Ga bond length to the shared Ga atom reduces to 2.640 Å. A further reduction in the bond length occurs for Bi clusters. For example, the average Bi-Ga bond length to the shared Ga atoms is 2.640 Å for a cluster of type 2. These trends are similar to those reported by experimental study,¹⁴ where a reduction in the bond lengths is observed for pairs and clusters. The x-ray absorption measurements indicated average bond length d_{av} values of 2.627, 2.621, and 2.619 Å for isolated, pairs, and clusters of Bi atoms.

Figure 7 shows the calculated fractional GaAs VBE Γ character for all seven of these nearest-neighbor environments. We recall in Fig. 7(b) that inclusion of a single Bi atom results in the mixing of a small amount ($\approx 2\%$) of the GaAs VBE Γ character into alloy states in the VB. Similar weak interactions can be seen in Figs. 7(c) and 7(e) for the cases where two and three isolated Bi atoms are incorporated in the alloy. In these cases, a large fraction [96% in Fig. 7(c) and 95% in Fig. 7(e)] of $G_{\Gamma}(E)$ again resides on the highest alloy valence

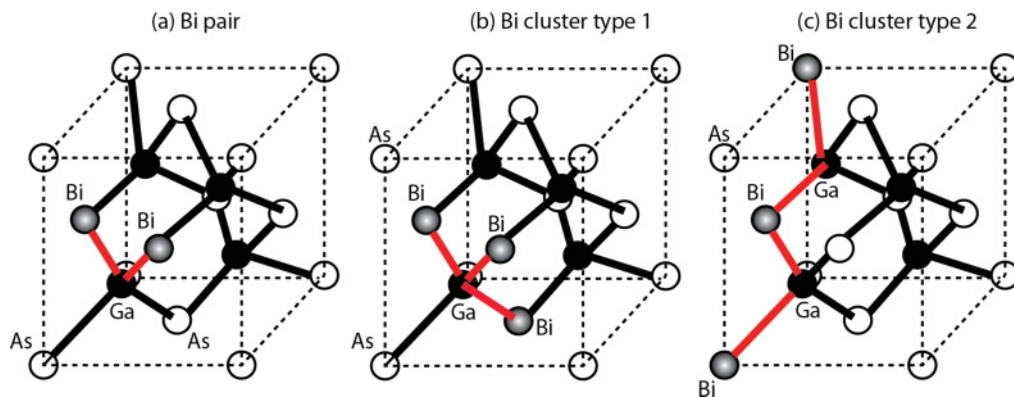


FIG. 6. (Color online) Three different Bi nearest-neighbor environments are used in our study of pairing and clustering effects: (a) a single Bi pair (i.e., an isolated Ga atom having two Bi nearest neighbors), (b) a cluster of Bi atoms is placed inside the supercell such that a single Ga atom has three Bi nearest neighbors (cluster type 1), and (c) a cluster of Bi atoms containing three Bi atoms in the form of a Bi-Ga-Bi-Ga-Bi chain. In this configuration, two Ga atoms have two Bi nearest neighbors (cluster type 2). Note that the nearest-neighbor environments are depicted here in their unrelaxed configurations. The bonds in the red color indicate the Bi pair and cluster connecting bonds.

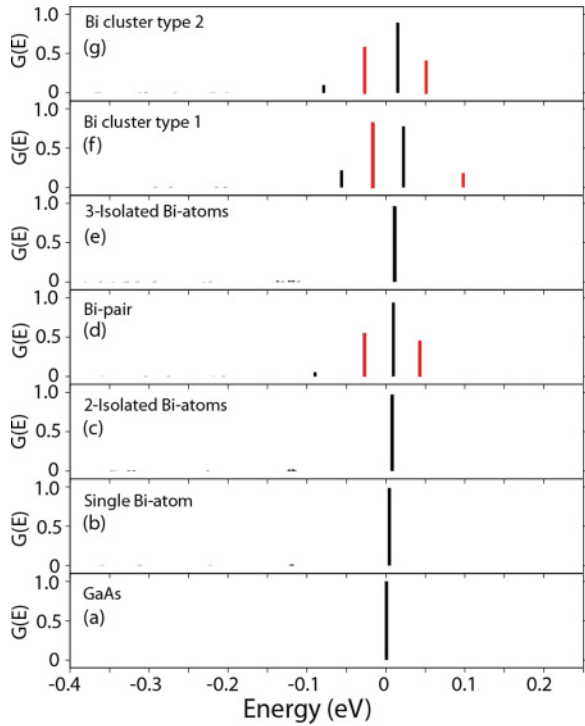


FIG. 7. (Color online) Combined fractional HH/LH Γ character for a series of disordered $\text{Ga}_{2048}\text{Bi}_M\text{As}_{2048-M}$ supercells for several different nearest-neighbor environments. The zero of energy is taken at the GaAs VBE.

state, with the remaining 4–5% distributed over a number of lower valence levels.

Turning to the Bi pair in Fig. 7(d), the Γ character is in this case distributed over four states, which form two interacting, anticrossing pairs (indicated by red and black bars). One of the pairs shown with the black color bars ($\approx 5.3\%$ weight at -90 meV and $\approx 94\%$ at 10 meV) behaves in a very similar way to the pair of states associated with isolated Bi atoms in Figs. 7(b) and 7(c), while the second pair (red bars) behaves quite differently, with $\approx 55\%$ Γ character on the lower state at -27 meV and $\approx 44\%$ Γ character on the upper state at 43 meV, associated with a Bi pair-related defect level just above the host matrix VBE. We can understand the behavior of these defect states based on interactions between the resonant states associated with two isolated Bi atoms. The formation of the Bi pair breaks the T_d symmetry about each Bi site, lifting the fourfold degeneracy of the Bi-related localized states to give a pair of twofold-degenerate states, one of which has a small interaction and the other a large interaction with Bi states on the neighboring Bi site. The interaction between the two Bi states with large overlap then gives rise to the defect level, which we calculate to be in the gap, similar to the behavior of the N-N pair state in GaAs,^{47,48} while the interaction between the other two sets of Bi states gives the resonant level calculated to be 90 meV below the host matrix VBE.

A similar analysis holds for the two types of Bi cluster considered. The type-2 cluster (chain of 3 Bi atoms) has a very similar spectrum to the Bi pair, with a stronger interaction between the lower defect and the VBE states than in the pair case, and with the higher defect state being slightly

deeper in the energy gap. We estimate that the energy level of the Bi defect state (E_{Bi}) is 10 , 8 , and 17 meV above the GaAs VBE for the Bi pair and the clusters of types 1 and 2, respectively. The lower defect state is shifted to -48 meV in the presence of a type-1 cluster, where one Ga atom has 3 Bi neighbors. Overall, the results follow similar trends to those found previously for N-related defect clusters in GaAs, where the defect levels tended to move deeper into the GaAs energy gap with increasing cluster size.

Table IV summarizes the calculated effect of the different Bi configurations on the lowest conduction band energy E_c , the top two valence bands E_{v1} and E_{v2} , and the spin-split-off band E_{SO} . Also shown in parentheses below each energy are the calculated change in energy for the band (per % Bi incorporation, relative to the corresponding GaAs band edge) as well as the overlap of the state with the corresponding unperturbed GaAs state. We see from these calculations that E_c and E_{SO} are both largely insensitive to the nearest-neighbor environment in the Bi-containing supercells. The conduction band exhibits a decrease of 28 meV per % Bi, which is linear in Bi composition, and retains a 99.9% overlap with the GaAs CBE for all Bi configurations considered. Thus, the variation in the conduction band and spin-split-off energies with increasing Bi composition can be well explained in terms of conventional alloy models, irrespective of disorder in the form of Bi pairs and clusters in the alloy. We note that unexpectedly large values have been deduced for the conduction band edge mass in $\text{GaBi}_x\text{As}_{1-x}$ alloys for $x \leq 6\%$.⁴⁹ Further studies are required to identify the cause of the anomalous CBE mass values deduced experimentally: our calculations indicate that it should be possible to describe the CBE mass in randomly disordered $\text{GaBi}_x\text{As}_{1-x}$ using conventional alloy models.

C. Electronic structure of disordered $\text{Ga}_{2048}\text{Bi}_M\text{P}_{2048-M}$ supercells

Having established the character of isolated Bi single, pair, and cluster impurity states in Secs. III A and III B, we now investigate the electronic structure of randomly disordered $\text{GaBi}_x\text{P}_{1-x}$ alloys, as we increase the number (M) of Bi atoms in a $\text{Ga}_{2048}\text{Bi}_M\text{P}_{2048-M}$ supercell. In order to trace the evolution of the highest valence states, we diagonalize the sp^3s^* Hamiltonian for the supercell and use the resulting alloy states to calculate the fractional Γ character $G_\Gamma(E)$ for the VBE [Eqs. (7) and (8)]. The calculated $G_\Gamma(E)$ spectra for a range of Bi compositions are shown in Fig. 8. We see in Fig. 8(b) for a single Bi atom in the supercell ($M = 1$, $x = 0.05\%$) that the amplitude of the unperturbed GaP VBE states is distributed over two levels, corresponding to E_- and E_+ , as previously discussed in Sec. III A.

In the supercells used in calculations containing $M \geq 10$ Bi atoms ($x \geq 0.49\%$), we see that the calculated splitting between the E_- and E_+ levels does not increase smoothly with increasing Bi composition. In addition, because of the reduced symmetry in these supercells and the inclusion of Bi pairs and clusters, the two highest valence states are no longer degenerate and we see an overall broadening of the spectra.

The pair and cluster states introduce higher-energy defect states, lying above the isolated Bi states in the energy gap, as can be seen at higher Bi composition in Fig. 8. The Bi defect

TABLE IV. Calculated effect of Bi isolated, pair, and clusters of atoms on the lowest conduction band, the highest two valence bands, and the spin-split-off band edges of $\text{Ga}_{2048}\text{Bi}_M\text{As}_{2048-M}$ supercells, including energy of given state and in parentheses the calculated change in energy for the band (per % Bi incorporation, relative to the corresponding GaAs band edge) as well as the overlap of the state with the corresponding unperturbed GaAs state.

Alloy composition	x (%)	E_{c1} (eV) (meV/% Bi, %)	E_{v1} (eV) (meV/% Bi, %)	E_{v2} (eV) (meV/% Bi, %)	E_{SO} (eV) (meV/% Bi, %)
Unperturbed GaAs	0	1.519 (0, 100)	0.000773 (0, 100)	0.000773 (0, 100)	-0.3518 (0, 100)
Single Bi-atom	0.049	1.5176 (28.57, 99.97)	0.00456 (77.28, 98.44)	0.004359 (73.18, 98.29)	-0.3521 (7.06, 99.95)
2-isolated Bi-atoms	0.098	1.5163 (27.55, 99.93)	0.008106 (74.82, 96.92)	0.007746 (71.15, 97.15)	-0.35244 (6.53, 99.94)
Bi-pair	0.098	1.5162 (28.57, 99.93)	0.04298 (430.68, 44)	0.009488 (88.92, 94.02)	-0.35244 (6.62, 99.34)
3-isolated Bi-atoms	0.146	1.5149 (28.08, 99.9)	0.01146 (73.2, 95.8)	0.01078 (68.51, 96.44)	-0.35273 (6.33, 99.75)
Bi-cluster type 1	0.146	1.5148 (28.76, 99.88)	0.09803 (666.14, 18.14)	0.0223 (147.44, 77.73)	-0.3526 (5.6, 99.75)
Bi-cluster type 2	0.146	1.5149 (28.08, 99.9)	0.05117 (345.18, 41.06)	0.01493 (96.96, 89.34)	-0.35273 (6.35, 99.64)

state distribution in $\text{GaBi}_x\text{P}_{1-x}$ then has a similar form to that observed in $\text{GaN}_x\text{P}_{1-x}$, where isolated N defect states are just below the GaP CBE, with defect states associated with N pairs and other cluster levels lying deeper in the energy gap.²¹

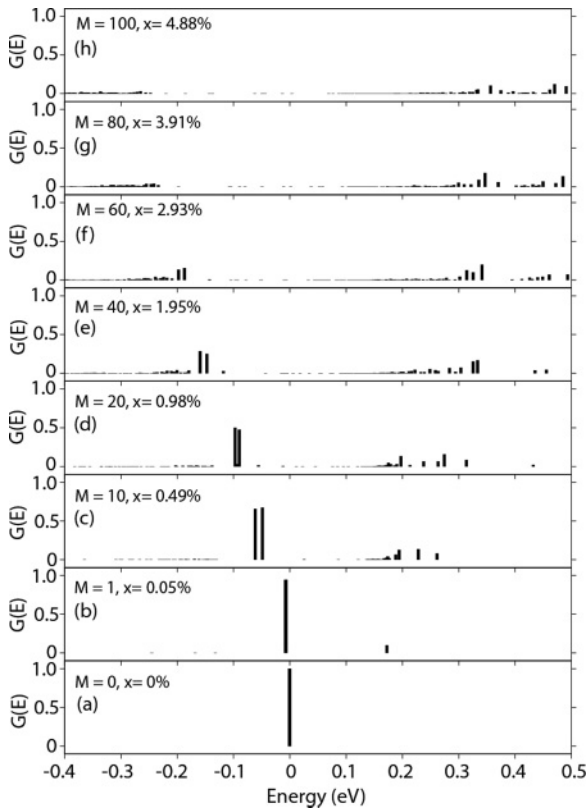


FIG. 8. Combined fractional HH/LH Γ character for a series of disordered $\text{Ga}_{2048}\text{Bi}_M\text{P}_{2048-M}$ supercells for several Bi compositions $x = \frac{M}{2048}$. The zero of energy is taken at the GaP VBE.

We can see from Fig. 8 that there is a general anticrossing interaction between the valence band states and the Bi defect states in the gap, with an increasing separation between the VB-related states (below 0 eV) and the Bi states in the gap (≥ 0.2 eV) with increasing Bi composition. However, because the gap defect levels are distributed over a range of energies, it is not possible to describe the band structure close to the energy gap using the two-level band anticrossing model of Eqs. (1) and (3). We showed previously for $\text{GaN}_x\text{P}_{1-x}$ that it is possible to treat the anticrossing interaction between the GaP host matrix Γ CBE and a distribution of N-related defect levels by treating explicitly the interaction between the GaP Γ conduction state and the full distribution of N defect levels.²¹ We see from Fig. 8 that this should also be the case in $\text{GaBi}_x\text{P}_{1-x}$. When the supercell only included isolated Bi atoms, then a clear anticrossing interaction was observed in Fig. 3, in agreement with Eq. (3). However, when the calculation includes a wider distribution of Bi environments (which is expected experimentally even for $x < 1\%$), then the two-level BAC model is no longer able to describe the observed evolution of the VBE states. We expect that a model similar to that used for $\text{GaN}_x\text{P}_{1-x}$ could also be used to describe the evolution of the band structure of $\text{GaBi}_x\text{P}_{1-x}$. We do not, however, pursue that further here.

D. Electronic structure of disordered $\text{Ga}_{2048}\text{Bi}_M\text{As}_{2048-M}$ supercells

1. Evolution of $\text{GaBi}_x\text{As}_{1-x}$ valence states with x

Figure 9 shows the calculated evolution of $G_{\Gamma}(E)$ for the highest valence states in a series of $\text{Ga}_{2048}\text{Bi}_M\text{As}_{2048-M}$ supercells, where the supercell energy spectrum is in each case projected onto the unperturbed GaAs valence-band-edge heavy-hole (HH) and light-hole (LH) wave functions [see Eqs. (7) and (8)]. To enable comparison with the results of our $\text{GaBi}_x\text{P}_{1-x}$ calculations, we consider identical Bi distributions within the supercells, with all P atoms replaced by As. For

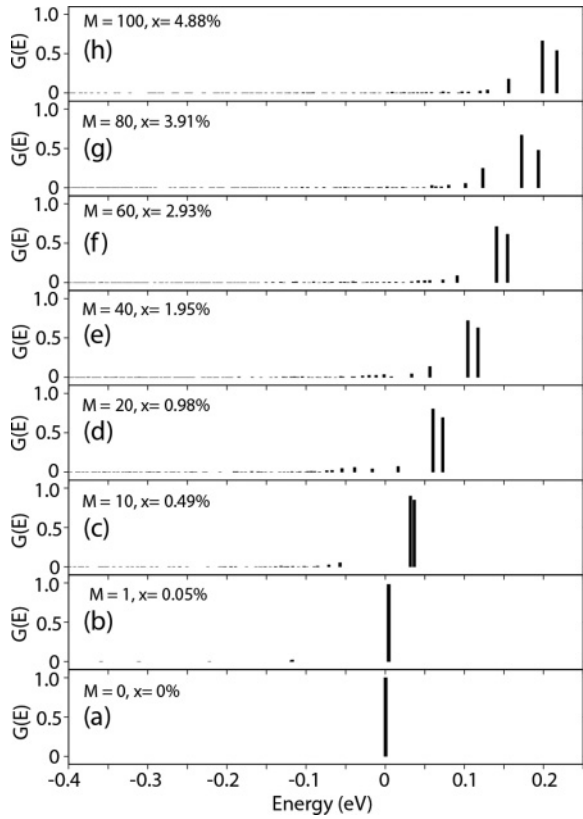


FIG. 9. Combined fractional HH/LH Γ character for a series of disordered $\text{Ga}_{2048}\text{Bi}_M\text{As}_{2048-M}$ supercells for several Bi compositions $x = \frac{M}{2048}$. The zero of energy is taken at the GaAs VBE.

reference, the lowest panel [Fig. 9(a)] shows the calculated $G_\Gamma(E)$ for an unperturbed $\text{Ga}_{2048}\text{As}_{2048}$ supercell, which is simply a single peak of unit amplitude, centered at the location of the $\text{Ga}_{2048}\text{As}_{2048}$ HH/LH energy levels. We observe in Fig. 9 that the calculated VBE energy shifts upward with increasing Bi composition x , and that the overall Γ character of the valence-band-maximum state decreases with increasing x , as expected from the BAC model of Eq. (3). The solid circles and triangles in Fig. 10 show how the calculated fractional Γ character $f_{\Gamma,v} = |\langle \psi_{v,0} | \psi_{v,1} \rangle|^2$ of each of the two highest valence states decreases with increasing Bi composition in the supercells considered. The solid line in Fig. 10 shows the expected variation in Γ using Eq. (3) with $E_{\text{HH/LH}} = 1.03 x$ eV, $E_{\text{Bi}} = -0.18$ eV, and $V_{\text{Bi}} = \beta\sqrt{x}$, with $\beta = 1.13$ eV. It can be seen that a good fit is obtained at low x , with the quality of the fit decreasing at higher values of x , as we move into a disordered regime in the alloy.

A resonant feature associated with the upper eigenvalue E_+ of the Hamiltonian (1) has been observed in PR measurements^{28,29} on $\text{GaN}_x\text{As}_{1-x}$ for $x > 0.2\%$, giving a relatively sharp feature until x reaches approximately 3%, beyond which composition the feature broadens and weakens when the resonant state becomes degenerate with the L -related CB levels.⁴⁴ It has not proved possible to observe such a feature at any composition in $\text{GaBi}_x\text{As}_{1-x}$, and this has led to controversy as to whether there is a VB-BAC interaction present in the alloy.¹⁷ It can be seen from Fig. 9 that the GaAs VBE character in $\text{GaBi}_x\text{As}_{1-x}$ is mixed into a wide range of

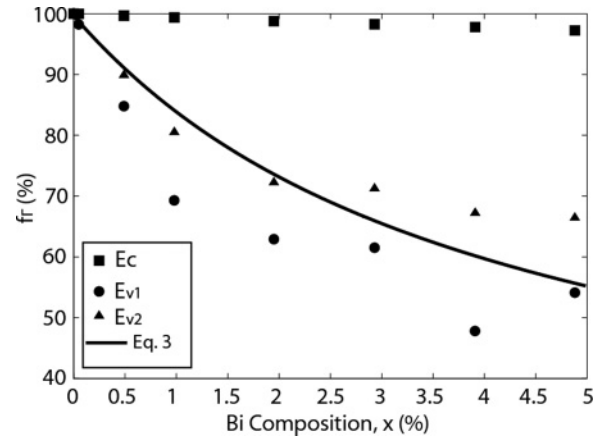


FIG. 10. Plot of fractional Γ character f_Γ [see Eq. (8)] of the lowest conduction band (E_c) and the highest two valence band (E_{v1} and E_{v2}) edges as a function of Bi composition. The solid line shows the valence band f_Γ character calculated using parameters in Eq. (3) extracted from tight-binding calculations of supercells containing isolated Bi atoms.

the alloy valence states so that, unlike in the $\text{GaBi}_x\text{P}_{1-x}$ case, no single state can be identified as the E_+ level in $\text{GaBi}_x\text{As}_{1-x}$. This strong mixing is to be expected because the width of the resonant level is proportional to the density of states.^{50,51} The large density of valence band states then explains the failure to observe an E_+ level in $\text{GaBi}_x\text{As}_{1-x}$ PR spectra.

2. Band gap and spin-orbit-splitting energies versus x

Figure 11 shows how the fractional Γ character of the SO band edge evolves with increasing Bi composition. As the Bi

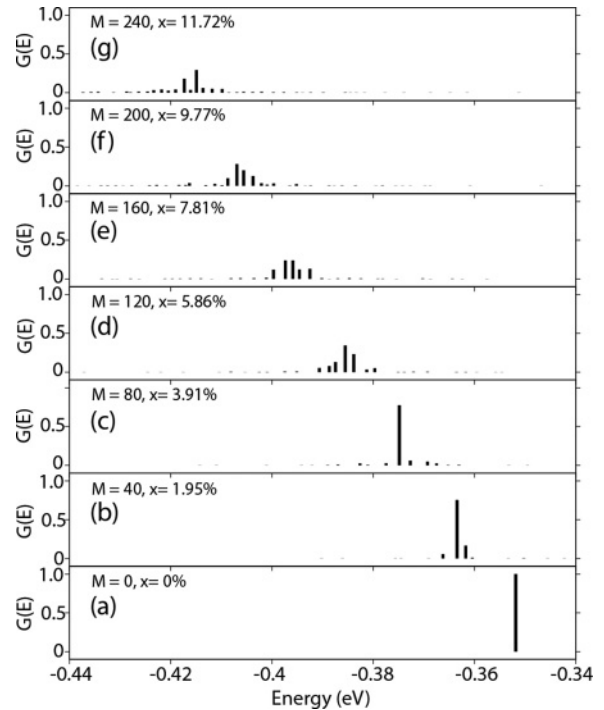


FIG. 11. Combined fractional SO Γ character for a series of disordered $\text{Ga}_{2048}\text{Bi}_M\text{As}_{2048-M}$ supercells for several Bi compositions $x = \frac{M}{2048}$.

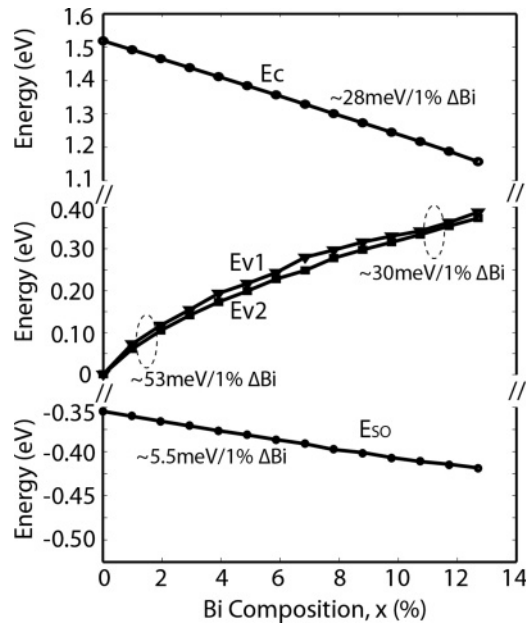


FIG. 12. The lowest conduction band edge E_c , the highest two valence band edges E_{v1} , E_{v2} , and the spin-split-off band E_{SO} energies are plotted as a function of Bi composition in $\text{GaBi}_x\text{As}_{1-x}$ supercells. The conduction band E_c edge decreases with a linear slope, changing by about 28 meV for every 1% increase in the Bi composition. The highest two valence band edges E_{v1} and E_{v2} exhibit a nonlinear change. For small Bi composition, the slope is large, i.e., 53 meV/1% Bi. For large Bi compositions, the slope decreases to about 30 meV/1% Bi. The spin-split-off band E_{SO} also decreases following a nearly linear slope of 5.5 meV/1% Bi.

composition increases, the Γ character spreads out over several states and it becomes unclear to choose a particular energy for E_{SO} . The values of the E_{SO} energies from Figs. 11(b)–11(g) are obtained by taking a weighted average of the energies with their corresponding Γ character as well as by picking the energies with the highest Γ character. The values from the two methods come out to be very close (within 0.1 meV of each other) and we deduce that both methods are equally good in this case. The Bi-induced disorder leads to a broadening of the projected Γ character $G_\Gamma(E)$ with increasing Bi composition, but no anticrossing behavior is observed in this broadened spectrum. Hence, the shift and broadening of the SO state projection are attributable to conventional alloying and disordering effects. For this reason, we conclude that our calculations do not support the existence of a Bi resonant state interacting with the SO band, as introduced in the $\mathbf{k} \cdot \mathbf{p}$ Hamiltonian of Alberi *et al.*⁷

Figure 12 shows the calculated variation of the lowest conduction, the two highest valence, and the spin-split-off band edge energies with increasing Bi composition x in the 4096-atom $\text{GaBi}_x\text{As}_{1-x}$ supercells. It can be seen that the calculated conduction band edge energy shifts down linearly by about 28 meV per % of Bi replacing As. The solid squares in Fig. 10 show that E_c retains $\geq 97\%$ GaAs conduction band Γ character for $x \leq 5\%$. With a linear decrease in the energy of E_c and the Γ character remaining close to 100%, we conclude that the evolution of the conduction

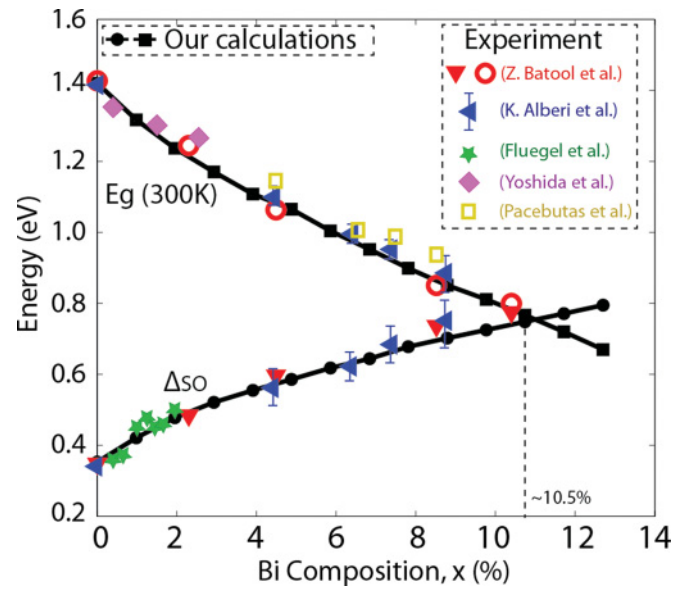


FIG. 13. (Color online) The band gap E_g and spin-orbit-splitting Δ_{SO} energies plotted as a function of Bi composition in 4096-atom $\text{GaBi}_x\text{As}_{1-x}$ alloy supercells. The solid circles and squares show the calculated data from our model. The triangles and open circles indicate the measured PR data from experiment [Batool *et al.* (Ref. 11)]. Four other sets of experimental data are also included for broader comparison.

band states is also best described using a conventional alloy model.

An important feature of $\text{GaBi}_x\text{As}_{1-x}$ alloys is that, as the Bi composition increases, the decreasing band gap $E_g = E_c - E_{v1}$ and the increasing spin-orbit-splitting energy $\Delta_{SO} = E_{v1} - E_{SO}$ results in a crossing of these two energies, with $E_g < \Delta_{SO}$ at higher Bi compositions. It has been suggested that this should lead at higher Bi compositions to a suppression of the dominant CHSH Auger recombination mechanism in $\text{GaBi}_x\text{As}_{1-x}$ where a conduction electron and heavy hole recombine to excite a hole to the split-off band from the heavy hole band. This would be highly beneficial for the design of high-efficiency lasers and semiconductor optical amplifiers (SOAs) operating at telecommunication and at longer wavelengths.¹³ Recent PR measurements¹¹ have confirmed a crossing of the energy gap and spin-orbit-splitting energies in bulk $\text{GaBi}_x\text{As}_{1-x}$ alloys for compositions above about $x = 10.5\%$.

Figure 13 plots the calculated band gap E_g and spin-orbit splitting Δ_{SO} as a function of Bi composition in 4096-atom $\text{GaBi}_x\text{As}_{1-x}$ supercells. The calculations were undertaken using the low-temperature $\text{GaBi}_x\text{As}_{1-x}$ band parameters presented here [$E_g(\text{GaAs}) = 1.519$ eV], and the CBE energy has then been shifted down by 92 meV for all Bi compositions, to fit to the GaAs energy gap at room temperature. Each data point shown in the figure is calculated by taking the average of three different random configurations of $\text{GaBi}_x\text{As}_{1-x}$. The results presented indicate that the decreasing band gap E_g and the increasing spin-orbit splitting do indeed lead to a crossover of E_g and Δ_{SO} at about 10.5% Bi composition, in agreement with PR measurements.¹³ For a broader comparison with other experiments, we have also included four sets of experimentally

measured band gap and spin-orbit-splitting values^{7,9,10,12} in Fig. 13 along with our calculated values. Our results exhibit a close match with the experimental data points over the entire composition range considered, confirming the validity of our model.

IV. CONCLUSIONS

In summary, we have developed a model based on the valence force field (VFF) and sp^3s^* tight-binding methods to study the dilute bismide alloys $\text{GaBi}_x\text{As}_{1-x}$ and $\text{GaBi}_x\text{P}_{1-x}$. Our results confirm that the evolution of the highest valence states in $\text{GaBi}_x\text{Y}_{1-x}$ ($Y = \text{P}, \text{As}$) can be described using a band anticrossing model. This has, until now, proved difficult to confirm experimentally because one of the key BAC features, the E_+ state observed in $\text{GaN}_x\text{As}_{1-x}$, is absent in $\text{GaBi}_x\text{As}_{1-x}$. We showed that this higher lying E_+ level, which has been identified in $\text{GaN}_x\text{As}_{1-x}$, can not be observed in $\text{GaBi}_x\text{As}_{1-x}$, due to the resonant levels being strongly broadened because of their interaction with the large density of valence states. In addition, we find that the presence of Bi pairs and clusters in a randomly disordered alloy introduce further defect levels, which also contribute to the suppression of the E_+ feature. We calculate that the experimentally observed strong band gap reduction is only partially explained through the valence band BAC interaction. We find that the conduction band edge energy also decreases with increasing Bi composition,

and that both band edge shifts contribute approximately equally (at large Bi compositions) to the reduction in the band gap energy of unstrained $\text{GaBi}_x\text{As}_{1-x}$ alloys. The computed dependence of band gap on Bi composition closely matches with experimental measurements. We calculate that the band gap and spin-orbit-splitting energies cross each other at 10.5% Bi composition in $\text{GaBi}_x\text{As}_{1-x}$, consistent with recent experimental measurements.¹³ It has been suggested that this crossover may eliminate the dominant CHSH Auger recombination loss mechanism in longer-wavelength photonic devices. Overall, we conclude that dilute bismide alloys open up new opportunities for band structure engineering and its application, with significant potential benefits for GaAs-based optical devices.

ACKNOWLEDGMENTS

This work was, in part, financed by the European Union Project No. BIANCHO (FP7-257974) and by Science Foundation Ireland (06/IN.1/190). C. A. Broderick acknowledges financial support from the Irish Research Council for Science, Engineering and Technology under the Embark Initiative (RS/2010/2766). NEMO 3-D simulator was developed by a number of researchers at Jet Propulsion Labs (JPL), Caltech, and Purdue University, whose work has been cited in the related references.^{30–32,52}

*usman@alumni.purdue.edu

- ¹M. Henini, *Dilute Nitride Semiconductors* (Elsevier, Amsterdam, 2005).
- ²I. A. Buyanova and W. M. Chen, *Physics and Applications of Dilute Nitrides* (CRC Press, Boca Raton, FL, 2004).
- ³A. Erol, *Dilute III-V Nitride Semiconductors and Material Systems: Physics and Technology* (Springer, Berlin, 2008).
- ⁴G. Pettinari, A. Polimeni, M. Capizzi, J. H. Blokland, P. C. M. Christianen, J. C. Maan, E. C. Young, and T. Tiedje, *Appl. Phys. Lett.* **92**, 262105 (2008).
- ⁵W. Shan, W. Walukiewicz, J. W. Ager, E. E. Haller, J. F. Geisz, D. J. Friedman, J. M. Olson, and S. R. Kurtz, *Phys. Rev. Lett.* **82**, 1221 (1999).
- ⁶A. Lindsay and E. P. O'Reilly, *Solid State Commun.* **112**, 443 (1999).
- ⁷K. Alberi, J. Wu, W. Walukiewicz, K. M. Yu, O. D. Dubon, S. P. Watkins, C. X. Wang, X. Liu, Y.-J. Cho, and J. Furdyna, *Phys. Rev. B* **75**, 045203 (2007).
- ⁸S. Tixier, S. E. Webster, E. C. Young, T. Tiedje, S. Francoeur, A. Mascarenhas, P. Wei, and F. Schiettekatte, *Appl. Phys. Lett.* **86**, 112113 (2005).
- ⁹V. Pačebutas, K. Bertulis, G. Aleksejenko, and A. Krotkus, *J. Mater. Sci.: Mater. Electron.* **20**, 363 (2009).
- ¹⁰J. Yoshida, T. Kita, O. Wada, and K. Oe, *Jpn. J. Appl. Phys., Part 1* **42**, 371 (2003).
- ¹¹Z. Batool, K. Hild, T. J. C. Hosea, X. Lu, T. Tiedje, and S. J. Sweeney, *Phys. Rev. B* 2011 (submitted).
- ¹²B. Fluegel, S. Francoeur, and A. Mascarenhas, S. Tixier, E. C. Young, and T. Tiedje, *Phys. Rev. Lett.* **97**, 067205 (2006).

- ¹³S. J. Sweeney, Z. Batool, K. Hild, S. R. Jin, and T. J. C. Hosea, *The potential role of bismide alloys in future photonic devices*, 13th International Conference on Transparent Optical Networks (ICTON) (IEEE, Stockholm, 2011), pp. 1–4.
- ¹⁴G. Ciatto, E. C. Young, F. Glas, J. Chen, R. Alonso Mori, and T. Tiedje, *Phys. Rev. B* **78**, 035325 (2008).
- ¹⁵M. Ferhat and A. Zaoui, *Phys. Rev. B* **73**, 115107 (2006).
- ¹⁶K. Alberi, O. D. Dubon, W. Walukiewicz, K. M. Yu, K. Bertulis, and A. Krotkus, *Appl. Phys. Lett.* **91**, 051909 (2007).
- ¹⁷H.-X. Deng, J. Li, S.-S. Li, H. Peng, J.-B. Xia, L.-W. Wang, and S.-H. Wei, *Phys. Rev. B* **82**, 193204 (2010).
- ¹⁸A. Janotti, S.-H. Wei, and S. B. Zhang, *Phys. Rev. B* **65**, 115203 (2002).
- ¹⁹Y. Zhang, A. Mascarenhas, and L.-W. Wang, *Phys. Rev. B* **71**, 155201 (2005).
- ²⁰P. R. C. Kent and A. Zunger, *Phys. Rev. B* **64**, 115208 (2001).
- ²¹C. Harris, A. Lindsay, and E. P. O'Reilly, *J. Phys.: Condens. Matter* **20**, 295211 (2008).
- ²²A. Lindsay and E. P. O'Reilly, *Phys. Rev. Lett.* **93**, 196402 (2004).
- ²³E. P. O'Reilly, A. Lindsay, P. J. Klar, A. Polimeni, and M. Capizzi, *Semicond. Sci. Technol.* **24**, 033001 (2009).
- ²⁴C. A. Broderick, M. Usman, A. Lindsay, E. P. O'Reilly, *Tight binding analysis of the electronic structure of dilute bismide and nitride alloys of GaAs*, 13th International Conference on Transparent Optical Networks (ICTON) (IEEE, Stockholm, 2011), pp. 1–4.
- ²⁵E. P. O'Reilly, A. Lindsay, S. Tomić, and M. Kamal-Saadi, *Semicond. Sci. Technol.* **17**, 870 (2002).

- ²⁶F. A. Trumbore, M. Gershenson, and D. G. Thomas, *Appl. Phys. Lett.* **9**, 4 (1966).
- ²⁷E. P. O'Reilly and A. Lindsay, *J. Phys.: Conf. Ser.* **242**, 012002 (2010).
- ²⁸J. D. Perkins, A. Mascarenhas, Y. Zhang, J. F. Geisz, D. J. Friedman, J. M. Olson, and S. R. Kurtz, *Phys. Rev. Lett.* **82**, 3312 (1999).
- ²⁹P. J. Klar, H. Grüning, W. Heimbrod, J. Koch, F. Höhnsdorf, W. Stolz, P. M. A. Vicente, and J. Camassel, *Appl. Phys. Lett.* **76**, 3439 (2000).
- ³⁰G. Klimeck, F. Oyafuso, T. Boykin, R. Bowen, and P. von Allmen, *Comput. Model. Eng. Sci.* **3**, 601 (2002).
- ³¹G. Klimeck, S. S. Ahmed, H. Bae, N. Kharche, S. Clark, B. Haley, S. Lee, M. Naumov, H. Ryu, F. Saied, M. Prada, M. Korkusinski, T. B. Boykin, and R. Rahman, *IEEE Trans. Electron. Dev.* **54**, 2079 (2007).
- ³²G. Klimeck, S. S. Ahmed, N. Kharche, M. Korkusinski, M. Usman, M. Prada, and T. B. Boykin, *IEEE Trans. Electron. Dev.* **54**, 2090 (2007).
- ³³M. Usman, H. Ryu, I. Woo, D. S. Ebert, and G. Klimeck, *IEEE Trans. Nanotechnol.* **8**, 330 (2009).
- ³⁴M. Usman, S. Heck, E. Clark, P. Spencer, H. Ryu, R. Murray, and G. Klimeck, *J. Appl. Phys.* **109**, 104510 (2011).
- ³⁵M. Usman, Y.-H. Matthias Tan, H. Ryu, S. S. Ahmed, H. J. Krenner, T. B. Boykin, and G. Klimeck, *IOP Nanotechnol.* **22**, 315709 (2011).
- ³⁶N. Kharche, S. Kim, T. B. Boykin, and G. Klimeck, *Appl. Phys. Lett.* **94**, 042101 (2009).
- ³⁷G. P. Lansbergen, R. Rahman, C. J. Wellard, I. Woo, J. Caro, N. Collaert, S. Biesemans, G. Klimeck, L. C. L. Hollenberg, and S. Rogge, *Nat. Phys.* **4**, 656 (2008).
- ³⁸J. C. Slater and G. F. Koster, *Phys. Rev.* **94**, 1498 (1954).
- ³⁹I. Vurgaftman, J. R. Meyer, and L. R. Ram-Mohan, *J. Appl. Phys.* **89**, 5815 (2001).
- ⁴⁰S. Francoeur, M.-J. Seong, A. Mascarenhas, S. Tixier, M. Adamcyk, and T. Tiedje, *Appl. Phys. Lett.* **82**, 3874 (2003).
- ⁴¹O. L. Lazarenkova, P. von Allmen, F. Oyafuso, S. Lee, and G. Klimeck, *Appl. Phys. Lett.* **85**, 4193 (2004).
- ⁴²P. N. Keating, *Phys. Rev.* **145**, 637 (1966).
- ⁴³R. Martin, *Phys. Rev. B* **1**, 4005 (1970).
- ⁴⁴A. Lindsay and E. P. O'Reilly, *Phys. E (Amsterdam)* **21**, 901 (2004).
- ⁴⁵A. Lindsay and E. P. O'Reilly, *Solid State Commun.* **118**, 313 (2001).
- ⁴⁶A. Lindsay, S. Tomić, and E. P. O'Reilly, *Solid-State Electron.* **47**, 443 (2003).
- ⁴⁷X. Liu, M.-E. Pistol, L. Samuelson, S. Schwetlick, and W. Seifert, *Appl. Phys. Lett.* **56**, 1451 (1990).
- ⁴⁸F. Masia, G. Pettinari, A. Polimeni, M. Felici, A. Miriametro, M. Capizzi, A. Cristofoli, G. Bais, M. Piccin, S. Rubini, F. Martelli, A. Franciosi, P. J. Klar, K. Volz, and W. Stolz, *Phys. Rev. B* **73**, 073201 (2006).
- ⁴⁹G. Pettinari, A. Polimeni, J. H. Blokland, R. Trotta, P. C. M. Christianen, M. Capizzi, J. C. Maan, X. Lu, E. C. Young, and T. Tiedje, *Phys. Rev. B* **81**, 235211 (2010).
- ⁵⁰U. Fano, *Phys. Rev.* **124**, 1866 (1961).
- ⁵¹S. Fahy, A. Lindsay, H. Ouerdane, and E. P. O'Reilly, *Phys. Rev. B* **74**, 035203 (2006).
- ⁵²NEMO 3-D based open source tools are available at [https://nanohub.org/groups/nemo_3d_distribution].